

Mapping of permafrost on Vega Island, Antarctic Peninsula, using satellite images and aerial photography

EVGENIY ERMOLIN, HERNÁN DE ANGELIS, PEDRO SKVARCA
Instituto Antártico Argentino, Cerrito 1248, C1010AAZ Buenos Aires, Argentina

ABSTRACT. The work presented deals with detailed mapping of permafrost in Devil Bay, Vega Island, northeastern Antarctic Peninsula. Mapping of landforms and permafrost features within a periglacial plain was performed using high resolution visible satellite images and aerial photography. Two maps of permafrost were produced: one based on analysis and interpretation of visible satellite imagery and another on low-altitude aerial photography, both yielding similar results. The principles of morphogenesis were applied to map production, distinguishing both the syncryogenic and epicryogenic formations and each constitutive cryofacies. The interpretation of remote-sensing data allowed areas of occurrence of particular cryogenic processes to be defined. Remote sensing was found to be useful for permafrost mapping at both medium and large scales, and applicable for future extension to other regions in Antarctica.

INTRODUCTION

Polar regions are known to be extremely sensitive to climate change. Recent estimates of future impacts due to significant environmental changes (i.e. greenhouse warming) suggest that we should be aware of the increasing severity of changes in polar areas in the near future (Watson and others, 1996; Weller, 1998). The northeastern part of the Antarctic Peninsula (AP) is no exception and is currently undergoing rapid and significant changes (e.g. general glacier retreat, disintegration of the northern Larsen Ice Shelf (Rott and others, 1998) and a 1.5°C rise in air temperature during the last three decades (Skvarca and others, 1998)). Exposed land where ice-rich permafrost exists in Quaternary deposits is very rare in

Antarctica. However, frozen deposits with ground ice are widespread on northeastern AP, which is therefore a region of interest for permafrost studies in the Southern Hemisphere. Permafrost is a sensitive indicator of climatic change because of the latter's pronounced effects on the thermal regime, structure and morphology of both the permafrost and the active layer (Koster, 1994). Whereas permafrost research in the Arctic is relatively advanced, Antarctic permafrost still remains poorly known. In spite of its importance for understanding cryospheric changes, extensive mapping of permafrost areas in Antarctica is still lacking. This paper describes the mapping by remote sensing and field data of the permafrost features of a small ice-free plain located in Devil Bay (63°49' S, 57°20' W), Vega Island (VI), northeastern AP. The work has three main objectives: to demonstrate the potential of satellite images and aerial photography to study a permafrost area in AP; to discriminate the indicators in permafrost study, both direct and indirect; and to carry out the first stage in monitoring of active cryogenic landforms on VI, AP.

STUDY AREA

Vega Island is located on the northeastern tip of AP (Fig. 1). It has a maximum length of 32 km in the east–west direction and 17 km in the north–south direction. Of the total area of 268 km², 70% is covered by ice. Glacial conditions have been present in AP at least since the Miocene (Dingle and Lavelle, 1998), providing a frame for permafrost formation. The climate is of the dry subpolar type, with a mean annual temperature of around –4.5°C. Glaciers are mainly of polythermal type (Paterson, 1994), and most terminate in ice cliffs at the sea. The study area in Devil Bay is an ice-free plain located on the northern side of the island. It lies almost entirely at sea level, being constricted by three glacier margins and rock escarpments. On its 4.5 km² almost all types of periglacial Quaternary deposits are present.

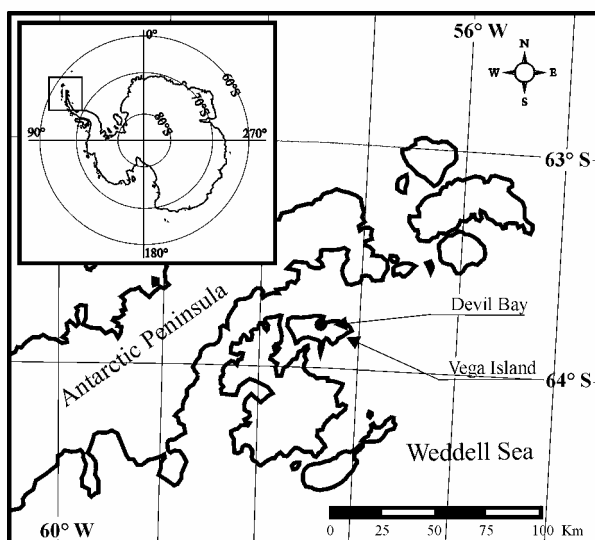


Fig. 1. Sketch map of northeastern AP showing location of the study area.

REMOTELY SENSED DATA AND METHODOLOGY

Four different sources were used to map permafrost features: a Système Probatoire pour l'Observation de la Terre 1, Haute Resolution Visible (SPOT 1 HRV) image (scene 730-482/0) of 23 March 1989; a Landsat 4 Thematic Mapper (TM) image (path/row 215/105) of 29 February 1988; a Landsat 7 Enhanced Thematic Mapper Plus (ETM+) image (path/row 216/105) of 21 February 2000; and a mosaic assembled with 35 mm standard camera photographs acquired during an aero-survey carried out on 27 January 2000. All images were georeferenced to the World Geodetic System 1984 ellipsoid, using Universal Transverse Mercator projection (zone 21 South). The images were tied to coastlines and other relevant features mapped in the field with kinematic differential global positioning system (DGPS).

Digital enhancements were performed on all satellite images to improve contrast. The advantages of combining near-infrared and visible Landsat TM bands were also exploited. The slight differences in spectral selectivity between TM and ETM+ sensors were not detected in our analysis. On Landsat images the combination of bands 4 and 2 (RGB: 4, 2, 2) together with linear enhancement proved useful in detecting the water bodies and separating the present ice-cored moraines from cryoturbated morainal debris. Furthermore, the combination of bands 7, 3 and 2 (RGB) on Landsat images allowed basalt outcrops and sedimentary deposits to be clearly distinguished. In these images the 30 m spatial resolution confines the identification to larger surface features. The panchromatic band 8 of the ETM+ sensor and the HRV of the SPOT sensor are particularly helpful because of their high spatial resolution (15 and 20 m, respectively), though limitations arise for permafrost mapping because of its broad spectral selectivity.

The hand-held aerial photographs were taken at an altitude of about 3000 m, corresponding to a 1:10 000 scale. Only seven photographs, each one covering a rectangle of 1700 m × 1200 m, were needed to compose the mosaic. The photographs were scanned to a pixel size of about 2 m. Finally, the mosaic was assembled by image registration to a geocoded database. Difficulties were found during mosaicking due to distortion of photographs introduced by the aircraft pitch and roll. These distortions could not be corrected since no flight parameters were recorded during the aero-survey. However, the matching inaccuracies were partly overcome by using a second-degree polynomial fit which was tied to a sufficient number of control points. The final product is a well-georeferenced mosaic, suitable for geomorphological mapping.

MAPPING OF PERMAFROST

To complement the remotely sensed database, fieldwork was carried out on Devil's Bay plain for ground-truth validation. Devil's Bay plain is the proglacial area of three glaciers, A–C (Figs 2 and 3). Remote sensing of key permafrost features such as icing glades, rock glaciers and thermokarst depressions suggests that the area lies in the zone of continuous permafrost. Weather records and field observations confirm this observation.

Applying the principles of morphogenesis (Spiridonov, 1970; Washburn, 1979), two maps were produced, one based on satellite images (Fig. 2) and the other on aerial photo-mosaic (Fig. 3). These principles establish the guidelines for

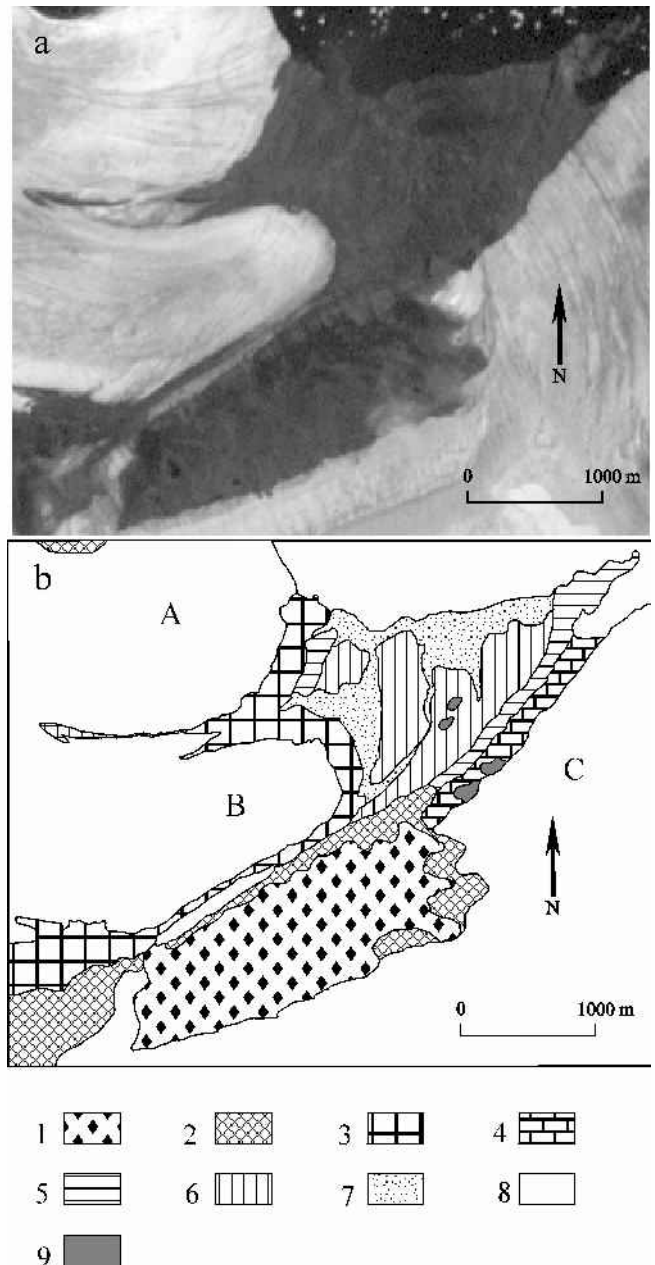


Fig. 2. (a) Section of Landsat 7 ETM+ image (band 8) of 21 February 2000, showing the study area in Devil Bay. (b) Map of permafrost derived from interpretation of satellite images. 1. Bedrock with cryoeluvium; 2. Bedrock frozen slope; 3. Present lateral and terminal moraine with buried ice; 4. Present bottom moraine with ground ice; 5. Holocene lateral moraine with buried ice; 6. Holocene bottom moraine with buried and ground ice; 7. Holocene and present fluvioglacial deposits with ground ice; 8. Glacier ice; 9. Marginal and thermokarst lakes.

permafrost mapping by discrimination of cryoformations and interpretation of cryogenic processes. Following these principles, two main cryoformations, epigenetic and syngenetic, were detected and mapped.

Epigenetic cryoformation consists of frozen deposits developed prior to the onset of regional permafrost conditions and occupies roughly 8% of the study area. This cryofacies is restricted to the 200 m high plateau south of the mapped area (Fig. 3). It was easily detected using a combination of Landsat bands 7, 3 and 2 (RGB) by applying a linear enhancement.

Syngenetic cryoformation comprises sedimentary deposits

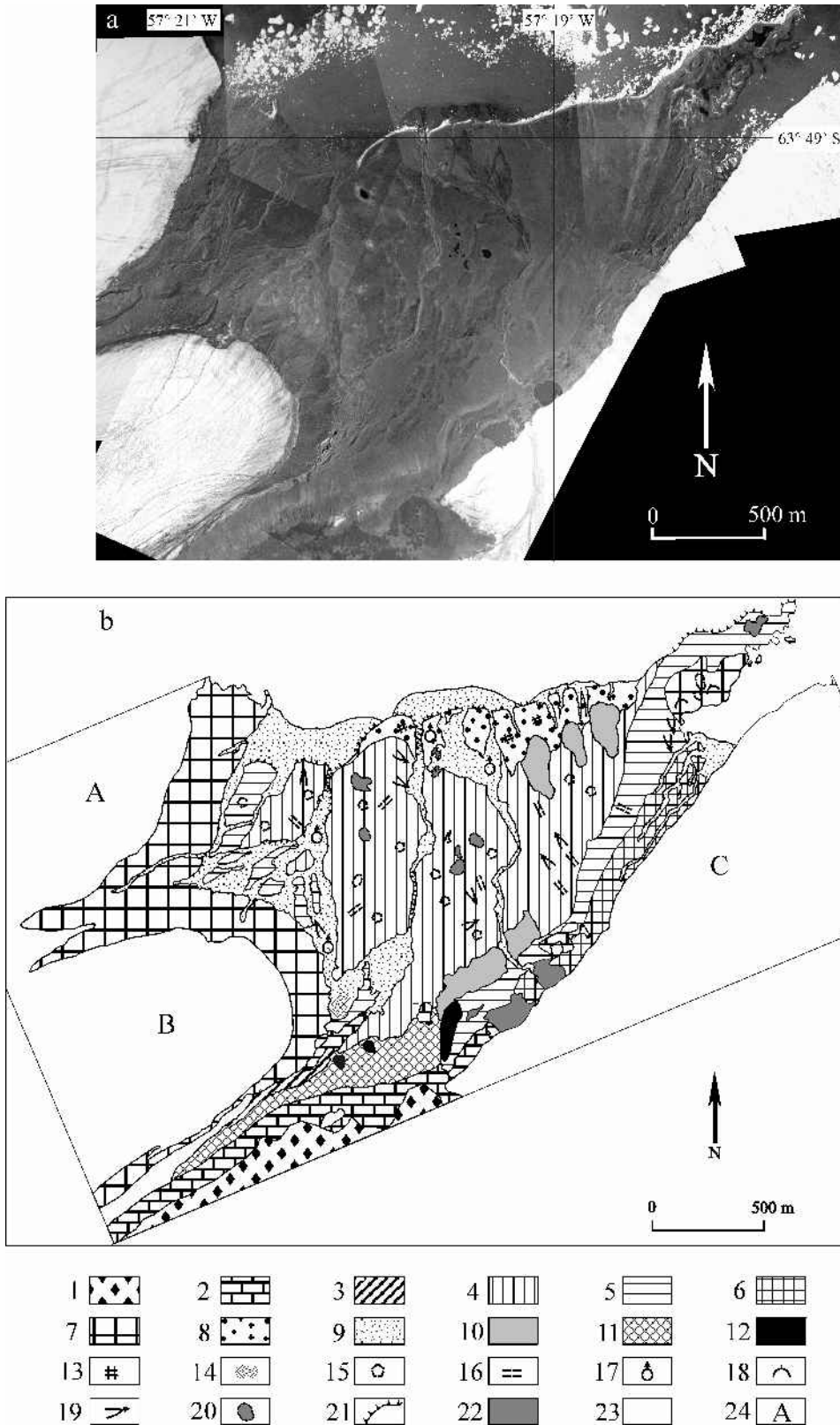


Fig. 3. (a) Mosaic of Devil Bay, assembled with aerial photography acquired on 27 January 2000. (b) Map of permafrost derived from photomosaic shown in (a). Facies of epigenetic cryoformation: 1. Cryoeluvium; 2. Bedrock. Facies of syngenetic cryoformation: 3. Late Pleistocene lateral moraine with buried ice; 4. Early Holocene bottom moraine; 5. Late Holocene lateral moraine with buried ice; 6. Present bottom moraine; 7. Present terminal moraine with buried ice; 8. Early Holocene fluvioglacial deposits (accumulation terrace); 9. Present fluvioglacial deposits (fluvioglacial plain and fan); 10. Solifluction deposits; 11. Slope deposits; 12. Rock glacier. Cryogenic phenomena: 13. Sand-wedge polygon; 14. Icing glade; 15. Sorted polygon; 16. Sorted stripe; 17. Frost jacking; 18. Frost blister; 19. Solifluction terrace and tongue; 20. Thermokarst depression; 21. Thermo-abrasion and thermo-erosion scarp; 22. Marginal and thermokarst lakes. Other: 23. Glacier ice; 24. Glacier nomenclature.

developed under permafrost conditions (Konishchev, 1969), which occupy around 92% of the study area. This cryoformation has been separated into different cryofacies

(Table 1). The most widespread cryofacies are lateral and bottom moraines, which can be clearly detected on aerial photographs as well as on Landsat images by using a

Table 1. Description of cryofacies of syngenetic formation derived from remote sensing and fieldwork

Cryofacies	Location	Cryogenic conditions	Geoindicators on images
Late Pleistocene lateral moraine	Moraine ridge of glacier B (130–180 m a.s.l.)	Buried ice. Depth 40 m, covering glacier and slope deposits	Ice exposed at different levels, landslides
Early Holocene bottom moraine	Central plain	Dominance of frozen ground with cement and pore ice (Ic 12–15%)	Thermokarst lake and depression, thermo-erosion scarp, frost sorting and sorted strip
Late Holocene lateral moraine	Ridge and residual moraine near edge of glaciers A and C	Frozen ground with pore and segregated ice (Ic 15–18%), area with buried ice < 50%	Thermokarst depressions, isolated solifluction forms and sorted ground
Present terminal moraine	Ridges of glaciers A and B	Buried ice > 95%	Ice outcrops, soil avalanches
Present bottom moraine	Snout of glacier C (150–200 m wide)	Frozen grounds with basal, pore and segregation ice	Surface separating fluvioglacial streams, eroded scarp
Rock glacier	Piedmont of plateau (70–100 m a.s.l.)	Ice core	Evidence of plastic deformation at axis and lower part
Present fluvioglacial deposits	Center of study area and near the coast	Cement and pore ice (Ic 10–15%)	Icing glade, frost jacking
Early Holocene fluvioglacial deposits	Fragments of accumulation terrace along coast	Pore and segregated ice (Ic 12–16%)	Homogeneous surface, polygonal wedges
Solifluction deposits	Central plain	Pore, basal and segregated ice (Ic 25–27%)	Evidence of movement, sorted ground
Slope deposits	Piedmont of plateau	Pore, basal and basal-layered ice (Ic 30–35%)	Stream channel, evidence of soil avalanche

Note: Ic, ice content.

specific band combination (RGB: 4, 2, 2). Fluvioglacial deposits are present in the proglacial area of glacier B and in the northern part of the mapped area, bordering the shoreline (Figs 2 and 3). Slope deposits were discriminated on TM and ETM+ images by selecting bands 7, 3, 2 (RGB). Rock glaciers are important indicators of permafrost occurrence. They usually originate from ice-cored moraines, mixed debris–snow avalanches or slope deposits (Corte, 1976; Hassinger and Mayewski, 1983). In our case, the detection of these landforms has limitations due to their small size and because their spectral signature is similar to those from which they originate (e.g. ice-cored moraine). Rock glaciers in the area could only be identified on air-photo mosaic.

Cryoturbated deposits are good geoindicators of buried ice (Black, 1976; Ermolin, 1986). In the study area, ice-rich permafrost shows evidence of soil creep and flow. Furthermore, thawing of buried or ground ice leads to development of thermokarst depressions and lakes. The monitoring of these zones is of special regional interest for comparative studies of neighbouring areas on AP.

MAP COMPARISON

The degree of detail obtained can be observed by comparing Figures 2 and 3. In satellite images general landforms and cryofacies were distinguished (Fig. 2), but their positive identification is limited to the larger ones. In some cases, however, it is observed that spatial resolution is not as important as the spectral selectivity. When discriminating between deposits with contrasting water content, even small (less than a pixel size) features with contrasting spectral responses can be detected on images (e.g. small water bodies). The high spatial resolution of SPOT and ETM+ (band 8) is very useful for detecting landforms even in small areas such as Devil's Bay plain. However, the spectral responses of both sensors could not be compared, due to the snow cover on the SPOT image. The main attribute of aerial photography is its high

spatial resolution, allowing direct identification of permafrost and other features. The lack of spectral selectivity had almost no effect on detection of morphological characteristics. The two maps show similar results, indicating that, given sufficient ground validation, it is possible to produce reliable maps of permafrost from satellite images.

CONCLUSIONS

Remote-sensing data were used for detailed mapping of permafrost in a proglacial plain located in Devil Bay. Although small, this region is a key site for permafrost research due to its unique assemblage of periglacial landforms. By applying the principles of morphogenesis, two maps were produced, based on high resolution visible satellite images and low-altitude aerial photography, respectively. Both maps show similar results. Digital enhancement and combination of specific spectral bands of Landsat TM and ETM+ sensors allowed most of the large-scale landforms and permafrost features to be detected. Due to much higher spatial resolution, direct identification of small features was only possible from aerial photography. The analysis and interpretation of the derived maps produced a general scheme of the cryogenic processes that occurred during the Holocene, allowing a comparison with present geocryological conditions. Long-term permafrost monitoring of key areas such as Devil's Bay plain is very important to assess the impact of AP regional atmospheric warming on the cryosphere. In addition, comparative studies of similar regions around the world will clarify the evolution trend of permafrost. Future extensive mapping of permafrost in northeastern AP could be based on high resolution visible satellite imagery, complemented with aerial photography and fieldwork in selected, localized areas.

ACKNOWLEDGEMENTS

We express our gratitude to T. Toconás, J. C. Quinteros and the

Twin Otter crew of Fuerza Aérea Argentina for their efficient support. Two anonymous reviewers provided useful comments. This work is a contribution to Glaciological Research Project in Antártica of Instituto Antártico Argentino–Dirección Nacional del Antártico.

REFERENCES

- Black, R. 1976. Periglacial features indicative of permafrost, ice and soil wedges. *Quat. Res.*, **6**(1), 3–26.
- Corte, A. E. 1976. Rock glaciers. *Biul. Peryglac.*, **26**, 175–197.
- Dingle, R. V. and M. Lavelle. 1998. Antarctic Peninsula cryosphere: Early Oligocene (c. 30 Ma) initiation and a revised glacial chronology. *J. Geol. Soc. London*, **155**(3), 433–437.
- Ermolin, E. 1986. Geoindikatory podzemnyi l'dov Pamira i Tianschanyia [Geoindicators of underground ice of Pamir and Tian-Shan]. In *Problemy geokriologicheskogo kartirovaniya* [Problems of geocryological cartography]. Yakutsk, Akademii Nauk SSSR. Institute of Permafrost Research, 17–24.
- Hassinger, J. M. and P. A. Mayewski. 1983. Morphology and dynamics of rock glaciers in southern Victoria Land, Antarctica. *Arct. Alp. Res.*, **15**(3), 351–368.
- Konishchev, V. N. 1969. K voprosu o formiravanií singeneticheskij merzlyj tolshch [An approach to the question of the formation of syngenetic frozen masses]. In *Problems of cryolithology. Vol. 1*. Moscow, Moscow University, 13–23.
- Koster, E. 1994. Global warming and periglacial landscapes. In Roberts, D., ed. *The changing global environment*. Oxford and Cambridge, Blackwells, 127–149.
- Paterson, W. S. B. 1994. *The physics of glaciers. Third edition*. Oxford, etc., Elsevier.
- Rott, H., W. Rack, T. Nagler and P. Skvarca. 1998. Climatically induced retreat and collapse of northern Larsen Ice Shelf, Antarctic Peninsula. *Ann. Glaciol.*, **27**, 86–92.
- Skvarca, P., W. Rack, H. Rott and T. Ibarzábal y Donángelo. 1998. Evidence of recent climatic warming on the eastern Antarctic Peninsula. *Ann. Glaciol.*, **27**, 628–632.
- Spiridonov, A. I. 1970. *Osnoviy obshchey metodiki polyevyij geomorfologicheskij issledovaniy i geomorfologicheskovo kartografirabaniya* [Basic methods of field geomorphological research and geomorphological mapping]. Moscow, Izdatel'stvo "Vyschaya shkola".
- Washburn, A. L. 1979. *Geocryology: a survey of periglacial processes and environments*. London, Edward Arnold.
- Watson, R. T., M. C. Zinyowera, R. H. Moss and D. J. Dokken. 1996. *Climate change 1995. Impacts, adaptations and mitigation of climate change: scientific-technical analysis contributions of Working Group II to the second assessment report of the Intergovernmental Panel on Climate Change*. Cambridge, etc., Cambridge University Press.
- Weller, G. 1998. Regional impacts of climate change in the Arctic and Antarctic. *Ann. Glaciol.*, **27**, 543–552.